Synthesis and Characterization of Some Reversible Iron(II) Dioxygen Carriers of Lacunar Macrobicyclic Ligands and Their Reactivities with Dioxygen

Norman Herron, L. Lawrence Zimmer, Joseph J. Grzybowski, Dennis J. Olszanski, Susan C. Jackels, Robert W. Callahan, James H. Cameron, Gary G. Christoph, and Daryle H. Busch*

Contribution from the Department of Chemistry, The Ohio State University, Columbus, Ohio 43210. *Received February 11, 1983*

Abstract: The preparation of a new family of iron(II) complexes with macrobicyclic ligands is described. These complexes contain a persistent protected void (lacuna) in the vicinity of one of the axial ligation sites of the metal ion, as shown by two X-ray crystal structures. [Chloro(2,12,14,20-tetramethyl-3,11,15,19,22,26-hexaazatricyclo[11.7.7.1^{5,9}]octacosa-1,5,7,9-(28),12,14,19,21,26-nonaene-κ^4N)iron(II)] chloride–2methanol crystallizes in the monoclinic space group $P2_1$, a = 10.606 (2) Å, b = 24.656 (3) Å, c = 10.132 (2) Å, β = 79.79 (2)°, and [chloro(2,3,11,12,14,20-hexamethyl-3,11,15,19,22,26-hexaazatricyclo[11.7.7.1^{5,9}]octacosa-1,5,7,9(28),12,14,19,21,26-nonaene-κ^4N)iron(II)] hexafluorophosphate crystallizes in the triclinic space group $P\bar{1}$, a = 8.575 (1) Å, b = 13.788 (2) Å, c = 14.383 (2) Å, α = 84.15 (1)°, β = 76.32 (1)°, γ = 104.80 (1)°, and both were solved by the heavy atom method to R = 5.7, 6.6% and R_w = 7.9, 8.5%, respectively, for $I > 3\sigma I$ data. Both structures confirm the presence of a lacuna but of dramatically different shape and steric requirements. This cavity may accommodate a small ligand such as dioxygen, and in favorable cases the complex can react reversibly with O_2 to produce dioxygen-carrying behavior. The oxygen-binding behaviors of a large number of the iron(II) species have been investigated spectrophotometrically. The strength and longevity of the reversible dioxygen-binding behaviors have been quantified and found to depend in large measure on the temperature (solution) and the steric design of the protective lacuna. In particular, a sterically demanding complex has been evolved which reversibly binds O_2 at room temperature in partially aqueous solvents. In certain anhydrous solvents this remarkable complex shows only slight evidence for autoxidation to iron(III) over extended periods. Characterization data are presented for all new complexes.

Introduction

The controlled interaction of dioxygen with iron(II) complexes in a reversible manner analogous to that of the hemoproteins, myoglobin, and hemoglobin has been an elusive goal for transition-metal coordination chemists for many years. Since the earliest claims of Kunz and Kress[1] in 1927 until 1973 no confirmed examples of reversible dioxygen binding by a synthetic iron(II) system existed, despite considerable activity in the area.[2] In 1973, however, two groups succeeded in their pioneering work on the generation and characterization of iron(II) dioxygen complexes. Baldwin's group made use of a sterically restricted iron(II) complex of a 14-membered unsaturated macrocycle in the belief that the steric bulk attached to the macrocycle periphery would serve the function of the globin portion of myoglobin and prevent irreversible oxidation of the metal ion occurring via μ-peroxo dimer formation.[3] The approach proved moderately successful in that the complex appeared (spectrophotometrically) to reversibly bind dioxygen in dry toluene at −80 °C. However, at −50 °C the complex irreversibly oxidized with a half-life of minutes. Following the same approach, Collman's and other groups developed sterically encumbered porphyrin complexes, e.g., the well-known picket-fence porphyrin,[4] which functioned as excellent reversible O_2 carriers even at room temperature, although only in nonaqueous solvents. It is perhaps not surprising, in light of the relative successes of these two approaches to dioxygen binding, that while a rash of porphyrin-based model systems have been developed since that time,[5] totally synthetic non-porphyrin complexes have been essentially ignored.

Reversible dioxygen binding by metal complexes is of great importance not only to biochemistry but also to industry where facilitated dioxygen transport using stable dioxygen carriers may represent an energy-efficient method of generating dioxygen-enriched air for synthetic fuel applications.[6] Therefore, a review of the current state of knowledge concerning reversible iron(II) dioxygen complex formation, with a view toward designing an iron complex capable of performing this function, reveals the following points: (1) Vogt has suggested[7] that one of the prime requirements is an iron(II/III) redox couple in a specific range such that if the divalent iron is too easily oxidized, irreversible electron transfer will occur, while at the other extreme no interaction will occur between Fe(II) and O_2; (2) the two conceptually simplest modes of autoxidation of iron dioxygen complexes involve (a) μ-peroxo dimer formation[8] and (b) proton-promoted superoxide expulsion following irreversible electron transfer from iron(II) to the coordinated dioxygen.[9] Prevention of these two processes is essential if reversible O_2 carrying is to be achieved. As already indicated above, steric factors within the iron complex may be used to control μ-peroxo dimer formation. Irreversible electron transfer, on the other hand, involves a charge separation, and therefore the transition state should be stabilized by polar solvent molecules. Prevention of autoxidation by this route should be possible by constructing ligands that prevent access of solvent or protons to the coordinated O_2 by burying it deep within lyophobic residues as occurs in the natural systems.

With this background we have sought to develop complexes of structure I (Figure 1) as totally synthetic (non-porphyrin) heme

(1) Kunz, K.; Kress, A. J. *Chem. Ber.* **1927**, *60*, 367.
(2) Larkworthy, L. F. *J. Chem. Soc.* **1961**, 4025. Drake, J. F.; Williams, R. J. P. *Nature (London)* **1958**, *182*, 1084. Davies, R. C. Ph.D. Thesis, Wadham College, Oxford, 1963.
(3) Baldwin, J. E.; Huff, J. *J. Am. Chem. Soc.* **1973**, *95*, 5257.
(4) Collman, J. P.; Gagne, R. R.; Halbert, T. R.; Marchon, J. C.; Reed, C. A. *J. Am. Chem. Soc.* **1973**, *95*, 7868.
(5) Almog, J.; Baldwin, J. E.; Huff, J. *J. Am. Chem. Soc.* **1975**, *97*, 227. Traylor, T. G.; Campbell, D.; Tsuchiya, S. *Ibid.* **1979**, *101*, 4748. Traylor, T. G.; Mitchell, M. J.; Tsuchiya, S.; Campbell, D. H.; Stynes, D. V.; Koga, N. *Ibid.* **1981**, *103*, 5234.
(6) Stewart, R. F.; Estep, P. A.; Sebastian, J. J. S. *U.S. Bureau of Mines Information Circ.* **1959**, *No. 7906*. Adduci, A. J. *Abstr. Pap.–Am. Chem. Soc.* **1975**, *170th*. Burke, D. P. *Chem. Week* **1980**, *127* (2), 18.
(7) Vogt, L. H., Jr.; Faigenbaum, H. M.; Wiberly, S. E. *Chem. Rev.* **1963**, *63*, 269.
(8) Chen, D. G.; Del Gaudio, J.; LaMar, G. N.; Balch, A. L. *J. Am. Chem. Soc.* **1977**, *99*, 5486. Sadasivan, N.; Eberspaecher, H. I.; Fuchsman, W. H.; Caughey, W. S. *Biochemistry* **1969**, *8*, 534.
(9) Sligar, S. G.; Lipscomb, J. D.; Debrunner, P. G.; Gunsalus, I. C. *Biochem. Biophys. Res. Commun.* **1974**, *61*, 290. Gilmour, A. G.; McAuley, A. *J. Chem. Soc. A* **1970**, 1006.

0002-7863/83/1505-6585$01.50/0

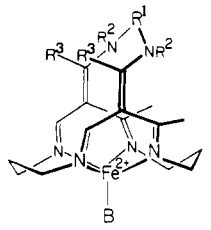

Figure 1. Representation of the lacunar complexes I emphasizing the presence of a cavity over one axial site of the iron(II).

protein models. Our attention was first drawn to this class of complex because $E_{1/2}$ for the Fe^{2+}/Fe^{3+} couple lies close to those of hemoglobin and myoglobin.[10] In addition to the persistent void or lacuna present in these structures,[11,12] the complexes are also characterized by tremendous flexibility in design.[12] These properties make such complexes extremely attractive as heme protein models since electronic and steric properties associated with small ligand coordination within the lacuna can be routinely and systematically varied in a closely controlled manner. This synthetic flexibility has been put to use in cobalt(II) complexes of I[13] where the O_2 affinity of the complexes may be controlled over a range of at least 10^5 $torr^{-1}$. The same relationships have been demonstrated for the formation of iron(II) carbonyl adducts of structure I.[14]

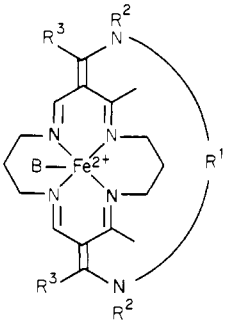

I

The present publication now seeks to detail the syntheses of a range of iron(II) lacunar complexes of structure I (Figure 1), to characterize them fully, and to describe the solution properties of these new iron(II) species. This report includes two X-ray crystal structures of such complexes which detail the dramatic effects of relatively minor substituent variations on the size and shape of the lacuna. The interaction of these iron(II) species with dioxygen is described in a manner showing the systematic variation in reversible binding that accompanies the systematic variation in structural parameters. Binding constants and, where feasible, thermodynamic parameters of dioxygen binding are presented for those species that interact reversibly with O_2. These results are related to electronic and structural parameters. The complex that is the most striking success to date in terms of longevity of reversible dioxygen-carrying ability is fully described.

Experimental Section

Materials. Solvents and reagents used in the synthesis of iron(II) complexes were reagent grade. Solvents were dried following recommended procedures[15] and distilled under N_2 before use.

Physical Measurements. ^1H NMR spectra were recorded on Varian EM390L continuous wave and Bruker WM300 fourier transform spectrometers at 90 and 300 MHz, respectively. Temperature on the former instrument was ambient at ~300 K and on the latter was controlled ±0.5 °C by a standard Bruker temperature controller. Solvents were deuterated as noted in text, and in all cases, shift measurements were made relative to internal tetramethylsilane at 0 ppm. Air sensitive samples were prepared in a glovebox and run immediately upon their removal from the inert atmosphere. The magnetic moment of iron(II) complexes was checked by the Evans method in a Wilmad coaxial capillary tube at 90 MHz and acetone reference in CD_3CN solvent. Temperature of this measurement was established using the standard methanol "thermometer" splitting between the CH_3 and OH signals.

Visible and ultraviolet spectra were obtained with a Cary 17D recording spectrophotometer while infra-red spectra were recorded as Nujol mulls between KBr disks with a Perkin-Elmer 283B recording spectrophotometer. Air-sensitive samples were prepared in an inert atmosphere and run immediately upon removal from the glovebox. Exposure of solutions of iron(II) complexes to dioxygen at various partial pressures was achieved with a series of calibrated rotameters (Matheson, E. Rutherford, NJ) to accurately mix dioxygen and dinitrogen standards. The gas mixture was first saturated with solvent vapor in a simple bubble cell held at the sample temperature followed by passage of the mixture through the sample solution in 1-cm quartz optical bubbling cells (Precision Cells, Inc., Hicksville, NY) equipped with a gas inlet and bubbling tube. The cell was thermostated (±0.3 °C) by using a NesLab or FTS constant-temperature circulation system, with methanol coolant flowing through a Varian variable-temperature double-jacketed cell holder within the nitrogen-flushed cell compartment of the Cary 17D spectrophotometer. The cell temperature was monitored with a calibrated copper-constantan thermocouple attached to the cell holder itself.

Dioxygen binding constants were obtained by the method of Stevens;[16] this involves monitoring electronic spectral changes as a function of dioxygen partial pressure at four different wavelengths across the spectrum with the Cary 17D spectrophotometer. The binding constant K_{O_2} was determined by using a nonlinear least-squares fit to the equation

$$A = A_0 + \frac{(\epsilon_{FeLBO_2} - \epsilon_{FeLB})K_{O_2}[FeLB]_o(P_{O_2})}{1 + K_{O_2}(P_{O_2})} \quad (1)$$

in which FeLB and $FeLBO_2$ represent the five coordinate precursor iron(II) complex (L = ligand, B = axial base/ligand) and its dioxygen adduct, respectively. A and A_0 represent the observed absorbance at a given partial pressure of $O_2(P_{O_2})$ and at $P_{O_2} = 0$, respectively.

Conductance measurements were obtained by using an Industrial Instruments (Andover, MA) Model RC 16B conductivity bridge with cell constant 0.11 cm^{-1} at 1000 Hz. Magnetic susceptibilities of the crystalline complexes were measured at room temperature by the Faraday method.

Electrochemistry was performed by using a Princeton Applied Research Corp. Potentiostat/Galvanostat Model 173 equipped with a Model 175 linear programmer and a Model 179 digital Coulometer. Current vs. potential curves were measured on a Houston Instruments Model 2000 XY recorder. All measurements were preformed in a glovebox under an atmosphere of dry nitrogen. The working electrode for voltammetric curves was a platinum disc, with potentials measured vs. an Ag^0/Ag^+ (0.1 M) reference. The working electrode was spun at 600 rpm by a synchronous motor for the rotating platinum electrode (RPE) voltamograms, and peak potentials were measured from cyclic voltamograms at a 50 mV/s scan rate. Half-wave potentials ($E_{1/2}$) were taken as the potential at one-half the height of the RPE voltamogram. The value $E_{3/4} - E_{1/4}$ also obtained from the RPE voltamogram was used as a measure of the reversibility of the couple ($E_{3/4} - E_{1/4}$ for a fully reversible one-electron couple is 60 mV). Elemental analyses were performed by Galbraith, Inc., Knoxville, TN.

Syntheses. The syntheses of the bridged ligands of I as their nickel(II) complexes and the removal of these ligands from nickel(II) have been previously described.[11,12] Elemental analyses for new compounds are

(10) Busch, D. H.; Pillsbury, D. G.; Lovecchio, F. V.; Tait, A. M.; Hung, Y.; Jackels, S. C.; Rakowski, M. C.; Schammel, W. P.; Martin, L. Y. *ACS Symp. Ser.* **1977**, *38*, 32–50. Subsequent studies showed that the example cited in this reference involves the dimeric bimetallic complex rather than the lacunar isomer claimed. However, $E_{1/2}$ for dimers and lacunar isomers is very similar.

(11) Schammel, W. P.; Mertes, K. B.; Christoph, G. G.; Busch, D. H. *J. Am. Chem. Soc.* **1979**, *101*, 1622. Busch, D. H.; Olszanski, D. J.; Stevens, J. C.; Schammel, W. P.; Kojima, M.; Herron, N.; Zimmer, L. L.; Holter, K. A.; Mocak, J. *Ibid.* **1981**, *103*, 1472. Busch, D. H.; Jackels, S. C.; Callahan, R. W.; Grzybowski, J. J.; Zimmer, L. L.; Kojima, M.; Olszanski, D. J.; Schammel, W. P.; Stevens, J. C.; Holter, K. A.; Mocak, J. *Inorg. Chem.* **1981**, *20*, 2834.

(12) Daszkiewicz, B. R. K.; Kojima, M.; Cameron, J. H.; Herron, N.; Chavan, M. Y.; Jircitano, A. J.; Coltrain, B. K.; Neer, G. L.; Alcock, N. W.; Busch, D. H., submitted for publication.

(13) Stevens, J. C.; Busch, D. H. *J. Am. Chem. Soc.* **1980**, *102*, 3285.

(14) Busch, D. H.; Zimmer, L. L.; Grzybowski, J. J.; Olszanski, D. J.; Jackels, S. C.; Callahan, R. W.; Christoph, G. G. *Proc. Natl. Acad. Sci. USA*, **1981**, *78*, 5919.

(15) Vogel, A. I. "A Textbook of Practical Organic Chemistry", 3rd ed.; Wiley: New York, 1966; 163–179.

(16) Stevens, J. C. Ph.D. Dissertation, The Ohio State University, Columbus, OH, 1979.

Table I. Analytical Data for New Iron(II) Lacunar Complexes I

R^1	R^2	R^3	yield	formula		% C	% H	% N	% Fe	% Cl
m-xylylene	H	CH_3	78%	$FeC_{26}H_{36}N_6Cl_2 \cdot 2CH_3OH$	calcd	53.94	7.11	13.48	8.96	11.37
					found	53.99	6.94	13.77	8.75	11.32
m-xylylene	CH_3	CH_3	72%	$FeC_{28}H_{40}N_6ClPF_6$	calcd	48.26	5.78	12.06		5.09
					found	48.22	5.93	12.00		5.01
m-xylylene	CH_3	C_6H_5	54%	$FeC_{40}H_{47}N_7P_2F_{12} \cdot 0.5C_2H_5OH$	calcd	49.52	5.10	9.82	5.59	
					found	49.27	4.95	9.62	5.60	
m-xylylene	$CH_2C_6H_5$	CH_3	48%	$FeC_{42}H_{51}N_7P_2F_{12}$	calcd	50.46	5.14	9.81	5.59	
					found	50.44	5.16	9.39	5.72	
m-xylylene	$CH_2C_6H_5$	C_6H_5	64%	$FeC_{52}H_{55}N_7P_2F_{12} \cdot 2.5CH_3OH$	calcd	54.41	5.43	8.16	4.65	
					found	54.28	5.17	8.25	4.54	
m-xylylene	CH_3	C_7H_{15}	60%	$FeC_{40}H_{62}N_6ClPF_6 \cdot 1.5H_2O$	calcd	53.96	7.31	9.44		
					found	53.81	7.38	9.69		
m-xylylene	CH_3	*p*-$OMeC_6H_4$	33%	$FeC_{40}H_{48}N_6O_2ClPF_6$	calcd	54.52	5.49	9.54	6.34	
					found	53.81	5.58	9.38	6.19	
m-xylylene	CH_3	*p*-ClC_6H_4	40%	$FeC_{38}H_{42}N_6Cl_3PF_6 \cdot CH_3OH$	calcd	50.76	4.99	9.11		
					found	50.20	5.14	8.95		
m-xylylene	CH_3	*p*-FC_6H_4	46%	$FeC_{38}H_{42}N_6ClPF_8 \cdot 0.3(FeCl_2 3CH_3OH)$	calcd	49.64	4.88	8.91	8.28	
					found	49.95	5.06	9.02	7.82	
$(CH_2)_4$	H	CH_3	50%	$FeC_{22}H_{36}N_6ClPF_6$	calcd	42.56	5.85	13.54	8.99	
					found	42.61	5.87	13.65	8.76	
$(CH_2)_4$	CH_3	CH_3	86%	$FeC_{24}H_{40}N_6ClPF_6$	calcd	44.41	6.17	12.95	8.64	
					found	44.30	6.09	12.90	8.72	
$(CH_2)_4$	CH_3	C_6H_5	93%	$FeC_{34}H_{44}N_6ClPF_6$	calcd	52.83	5.74	10.87	7.22	
					found	52.60	5.74	10.68	7.32	
$(CH_2)_5$	H	CH_3	71%	$FeC_{23}H_{38}N_6Cl_2$ 10% $ZnCl_4$ anion	calcd	51.25	7.11	15.59		
					found	51.27	7.13	15.65		
$(CH_2)_5$	CH_3	CH_3	23%	$FeC_{25}H_{42}N_6ClPF_6$	calcd	45.28	6.34	12.68	8.45	
					found	45.56	6.51	12.90	8.22	
$(CH_2)_5$	CH_3	C_6H_5	72%	$FeC_{35}H_{46}N_6ClPF_6$	calcd	53.41	5.89	10.68	7.10	
					found	53.36	5.89	10.78	7.33	
$(CH_2)_6$	CH_3	CH_3	78%	$FeC_{26}H_{44}N_6ClPF_6$	calcd	46.13	6.55	12.41	8.25	5.24
					found	45.99	6.45	12.30	7.94	5.14
$(CH_2)_6$	CH_3	C_6H_5	92%	$FeC_{36}H_{48}N_6ClPF_6 \cdot 2CH_3OH$	calcd	53.00	6.43	9.87	6.56	
					found	52.70	6.21	10.10	6.71	
$(CH_2)_6$	$CH_2C_6H_5$	C_6H_5	62%	$FeC_{48}H_{56}N_6ClPF_6$	calcd	60.48	5.92	8.82	5.86	
					found	60.56	6.02	8.84	6.12	
$(CH_2)_6$	H	CH_3	63%	$FeC_{24}H_{40}N_6ClPF_6$	calcd	44.42	6.21	12.95	8.61	
					found	44.38	5.93	12.66	8.89	
p-xylylene	H	CH_3	75%	$FeC_{26}H_{36}N_6ClPF_6$	calcd	46.69	5.43	12.56		5.30
					found	46.59	5.77	11.93		4.67
7-fluorenylidene	H	CH_3	68%	$FeC_{37}H_{48}N_6ClPF_6$	calcd	63.16	6.88	11.94	7.94	
					found	62.90	6.87	12.16	7.64	

given in Table I. All syntheses of iron(II) complexes were carried out under oxygen-free nitrogen in a Vacuum Atmospheres glovebox.

[Chloro(2,12,14,20-tetramethyl-3,11,15,19,22,26-hexaazatricyclo-[11.7.7.1^{5,9}]octacosa-1,5,7,9(28),12,14,19,21,26-nonaene-κ^4N)iron(II)] Chloride–2Methanol (I, R^1 = ***m*-Xylylene**; R^2 = H; R^3 = CH_3). To a solution of 1.0 g (1.2 mmol) of $[H_4(m\text{-}CH_2C_6H_4CH_2)(HNEthi)_2Me_2$-[16]tetraeneN$_4$]$(PF_6)_3Cl$[11] dissolved in 50 mL of acetonitrile were added 0.24 g (1.2 mmol) of bis(acetonitrile)iron(II) chloride[17] and 0.35 g (3.5 mmol) of triethylammine to yield a deep red solution. This solution was filtered through celite, stirred overnight, and the orange precipitate that formed was collected and dried in vacuo. This product may be recrystallized from methanol to yield large crystals of the dimethanol solvate suitable for X-ray analysis (yield, 0.5 g (78%)).

[Chloro(2,3,11,12,14,20-hexamethyl-3,11,15,19,22,26-hexaazatricyclo[11.7.7.1^{5,9}]octacosa-1,5,7,9(28),12,14,19,21,26-nonaene-κ^4N)iron(II)] Hexafluorophosphate (I, R^1 = ***m*-Xylylene**; R^2 = CH_3; R^3 = CH_3). One gram (1.1 mmol) of $[H_4(m\text{-}CH_2C_6H_4CH_2)(MeNEthi)_2Me_2$[16]tetraeneN$_4$]$(ZnCl_4)_2$[11] and 0.35 g (1.2 mmol) of bis(pyridine)iron(II) chloride[18] were slurried in 25 mL of methanol. Addition of 0.5 g (5 mmol) triethylamine produced an immediate deep red coloration and caused all solids to dissolve. Addition of 1.5 g of NH_4PF_6 in a minimum of methanol gave a clear red solution, which on standing overnight gives deep red crystals of the desired product, suitable for X-ray analysis (yield, 0.58 g (72%)).

[Chloro(2,3,10,11,13,19-hexamethyl-3,10,14,18,21,25-hexaazabicyclo[10.7.7]hexacosa-1,11,13,18,20,25-hexaene-κ^4N)iron(II)] Hexafluorophosphate (I, R^1 = $(CH_2)_6$; R^2 = CH_3; R^3 = CH_3). Two grams (2.3 mmol) of $[H_4((CH_2)_6(MeNEthi)_2)Me_2$[16]tetraeneN$_4$]$(PF_6)_3Cl$[11] and 0.75 g (2.6 mmol) of bis(pyridine)iron(II) chloride were slurried in 25 mL of acetonitrile. Addition of 1.0 g (10 mmol) of triethylamine produced a clear red solution, which was refluxed for 5 min, cooled, and filtered through celite. The solvent was removed and the residue dissolved in a minimum volume of hot methanol, which was stirred as it cooled. After the solution stirred for 10 min, deep red crystals of the desired complex may be filtered off and dried in vacuo. Further product may be obtained from the filtrate by slow addition of NH_4PF_6 saturated ethanol, which gives a powdery red precipitate (yield, 1.21 g (78%)).

All other iron(II) complexes reported in Table I were prepared by one of these three procedures or combinations thereof. Generally the last procedure was most successful. Yields are as quoted in Table I.

Crystal Data. (a) [Chloro(2,12,14,20-tetramethyl-3,11,15,19,22,26-hexaazatricyclo[11.7.7.1^{5,9}]octacosa-1,5,7,9(28),12,14,19,21,26-nonaene-κ^4N)iron(II)] Chloride–2Methanol (I, R^1 = ***m*-Xylylene**; R^2 = H; R^3 = CH_3). A deep red crystal from methanol was coated with epoxy resin and mounted (dimensions 0.25 × 0.25 × 0.15 mm) for examination on a Syntex P$\bar{1}$ four-circle automated diffractometer. The unit cell dimensions and their esd's were obtained from a least-squares fit to 15 high-angle reflections ($2\theta > 20°$) by use of Mo Kα graphite monochromatized radiation (λ = 0.71069 Å) at 293 K. Systematic absences, $0k0$, $k = 2n + 1$, and precession photographs indicated a monoclinic space group $P2_1$ or $P2_1/m$. Crystal data were as follows: $FeCl_2O_2N_6C_{28}H_{44}$, M_r 623, monoclinic space group $P2_1$ or $P2_1/m$, a = 10.607 (2) Å, b = 14.656 (3) Å, c = 10.132 (2) Å, β = 79.79 (2)°, V = 1550.2 (5) Å^3, T = 293 ± 1 K, d_m(bromoform/chloroform) = 1.34 g cm^{-3}, d_x = 1.34 g cm^{-3}, Z = 4, $\mu_{Mo\,K\alpha}$ = 6.95 cm^{-1}, $F(0,0,0)$ = 1320. Intensity data were collected by the ω–2θ scan technique with variable scan rate between 2.0 and 16.0 deg/min in the region $4° < 2\theta < 50°$. Ten check reflections were monitored periodically to follow the condition of the crystal in the X-ray beam and displayed no appreciable decay of intensity. A total of 6047 reflections (2874 independent and 1509 with $I > 3\sigma(I)$) were collected and used in structure determination. Lorentz and polarization corrections were applied, but no correction for absorption or extinction

(17) Hathaway, G. J.; Holah, D. G. *J. Chem. Soc.* **1964**, 2408.
(18) Long, G. J.; Whitney, D. L.; Kennedy, J. E. *Inorg. Chem.* **1971**, *10*, 1406.

was used because of the crystal size and low absorption coefficient.

(b) **[Chloro(2,3,11,12,14,20-hexamethyl-3,11,15,19,22,26-hexaazatricyclo[11.7.7.1^{5,9}]octacosa-1,5,7,9(28),12,14,19,21,26-nonaene-κ^4N)iron(II)] Hexafluorophosphate (I, R^1 = *m*-Xylylene; R^2 = CH$_3$; R^3 = CH$_3$).** A red crystal from acetonitrile/ethanol (0.11 × 0.21 × 0.29 mm) was coated with epoxy resin, mounted, and centered on the Syntex P$\bar{1}$ automated diffractometer. The unit cell dimensions and their esd's were obtained from a least-squares fit to 15 high-angle reflections ($2\theta > 20°$) by using graphite monochromatized Mo Kα radiation (λ = 0.71069 Å) at 200 ± 3 K. Precession photographs indicated a triclinic crystal system, space group *P*1 or *P*$\bar{1}$. Crystal data were as follows: $FeClPF_6N_6C_{28}H_{40}$, M_r 696.5, triclinic space group *P*1 or *P*$\bar{1}$, a = 8.575 (1) Å, b = 13.788 (2) Å, c = 14.383 Å, α = 84.15 (1)°, β = 76.32 (1)°, γ = 104.80 (1)°, V = 1573.6 (4) Å^3, T = 200 ± 3 K, d_m (benzene/bromoform) = 1.46 g cm^{-3}, d_x = 1.47 g cm^{-3}, Z = 2, $\mu_{Mo K\alpha}$ = 6.76 cm^{-1}, $F(0,0,0)$ = 724. Intensity data in the range $4° < 2\theta < 60°$ were collected by the ω-2θ scan technique with a variable scan rate between 2.0 and 16.0 deg/min. Ten check reflections were monitored every 190 reflections and remained constant throughout data collection. Of 12 956 measured reflections, 9230 were unique and 3042 had $I > 3\sigma(I)$. Lorentz, polarization, and absorption corrections were applied.

Solution and Refinement of Structures. Both data sets described above were subjected to analysis of E-statistics in order to evaluate the centricity of the space groups. I, R^2 = H, gave statistics most consistent with an acentric group and thus $P2_1$ was selected. I, R^2 = CH$_3$, gave statistics slightly more consistent with a centric group and so *P*$\bar{1}$ was selected (refinement was also attempted in *P*1 but with unsatisfactory results).

Both structures were solved by the heavy atom method and refined by the full-matrix least-squares method. In the least-squares procedure, the function minimized was $\sum w|F_o^2 - F_c^2|^2$, where $w = 1/\sigma^2(F_o^2)$. Atomic scattering factors were taken from "International Tables for X-ray Crystallography", Vol. IV, for H, C_{cov}, N, O, F, P, Cl, and Fe[19]. All calculations were carried out on an IBM 3170/165 computer in the Computer Center of The Ohio State University with CRYM crystallographic computing system.[20]

(a) I, R^2 = H. The coordinates of the iron(II) atom and one of the chlorine atoms were located in a sharpened Patterson map and the y coordinate of the iron atom was fixed at 0.25 cell units. Successive structure factor calculations and fourier maps allowed location of the remainder of the non-hydrogen atoms except for the methanol solvate. Refinement with isotropic thermal parameters was carried out to R_1 = 0.235 where the discrepancy indices are defined as $R_1 = \sum||F_o| - |F_c||/\sum|F_o|$, $R_w = (\sum w(F_o^2 - F_c^2)^2/\sum wF_o^4)^{1/2}$, and GOF = $(\sum w(F_o^2 - F_c^2)^2/(n_o - n_p))^{1/2}$. Electron density corresponding to the methanol solvates was found but refinement of their positions resulted in high thermal parameters indicating disorder. The populations of the methanol molecules were allowed to vary and approached values of 1.0. Refinement of all non-hydrogen atoms was completed with anisotropic thermal parameters; hydrogen atom positions were calculated after each least-squares cycle and were included in structure factor calculations but were not refined. At convergence, R_1 = 0.103, R_w = 0.092, and GOF = 1.33 on the basis of all 2874 reflections and R_1 = 0.057 and R_w = 0.079, for the 1509 $I > 3\sigma(I)$ data. A final difference fourier map indicated some residual electron density in the vicinity of the methanol molecules.

(b) I, R^2 = CH$_3$. The position of the iron(II) atom was found in a sharpened Patterson map, and the rest of the molecule, including the ordered hexafluorophosphate anion, was found from two Fourier maps. The structure was refined in the same manner as above with all non-hydrogen atoms anisotropic. The final discrepancy indices were R_1 = 0.154, R_w = 0.112, and GOF = 1.21 for all 9230 reflections and R_1 = 0.066 and R_w = 0.085, using only the 3042 reflections with $I > 3\sigma(I)$. A final difference map showed no peaks having electron density >0.6 e/Å^3.

Final positional parameters with their esd's for both structures and a list of observed and calculated structure factors are listed in the supplementary material. Bond lengths and angles are included in Table II.

Discussion

Synthesis and Characterization of New Iron(II) Complexes I. Reaction of the previously described[11,12] ligand salts of lacunar ligands I with a source of iron(II) chloride and triethylamine in acetonitrile or methanol solvent invariably leads to the generation of deep red, highly oxygen-sensitive solutions of the desired iron(II) lacunar complexes. Care must be taken, however, with complexes of ligands where R^2 = H, since a previous report[21] has already detailed the possible rearrangement process that these complexes can undergo to generate clathro-chelate structures. The proton at R^2 in these complexes may be induced to migrate to the γ carbon of the unsaturated chelate ring while the concomitantly formed imine group coordinates to the metal center. This undesired reaction may easily be controlled, however, by careful monitoring of temperature of the solvent and the careful exclusion of a large excess of base from the synthesis reaction, all as previously described.[14,21]

The desired red complexes may be readily obtained as crystalline materials by recrystallizing from acetonitrile/ethanol or methanol. The composition of the resultant material as shown by elemental analysis, Table I, appears to depend on the relative solubilities of the salts of the possible anions in solution. For example, most of the complexes crystallize as a chlorohexafluorophosphate mixed anion salt but several of the R^1 = *m*-xylylene derivatives crystallize as bis(hexafluorophosphate) salts. The dichloro- and chlorohexafluorophosphate salts have the chloride anion coordinated to the metal as an axial ligand while the bis(hexafluorophosphate) salts tend to have acetonitrile as the analogous axial ligand, vide infra. An alternative explanation for the occurrence of bis(hexafluorophosphate) salts in a few instances may be that in these complexes the two saturated six-membered chelate rings of the complexes are forced, sterically, to adopt boat conformations. This distortion from the normal chair configurations (see X-ray data below) would tend to crowd the axial chloride ion and perhaps cause it to be readily substituted by a smaller linear ligand, such as acetonitrile. That such distortion does indeed occur in the more heavily substituted complexes is evident from the X-ray structure of the nickel complex R^1 = *m*-xylylene, R^2 = benzyl, R^3 = phenyl,[12] which is reproduced below.

The infrared spectra of all of the iron complexes are unremarkable. Those with R^2 = H show a single N–H absorption in the 3200–3450 cm^{-1} region, usually at the upper end of this range and sharp, but the dichloride salts show a broader absorption at the lower end of the region indicative of hydrogen bonding to the chloride anion and/or solvent. The region between 1500 and 1650 cm^{-1} invariably contains two strong bands from the C=C and C=N stretches, the higher energy band being sharper and less intense than the other. The splitting between these two bands tends to increase as the bulk of substituents R^1, R^2, and R^3 increases; for example, the species with R^1 = *m*-xylylene, R^2 = H, and R^3 = CH$_3$ shows bands at 1620 and 1575 cm^{-1} whereas that with R^1 = *m*-xylylene, R^2 = benzyl, and R^3 = phenyl has bands at 1608 and 1530 cm^{-1}. In general, the separations between these two bands parallels that observed in the precursor nickel complex of the same ligand. Those bis(hexafluorophosphate) salt complexes having acetonitirle as the axial ligand (Table I) show a weak nitrile absorption at ~2310 cm^{-1}.

Magnetic moments have been determined for the new complexes and are tabulated in Table III. Solid-state magnetic moments at room temperature were determined by the Faraday method and are consistent with the presence of high-spin iron(II). The magnetic moments in solution were determined by the Evans ^{1}H NMR method[22] and again, at room temperature, are consistent with a high-spin configuration.

The molar conductances of several of the chlorohexafluorophosphate complexes, 1 mM in acetonitrile, range between 125 and 150 Ω^{-1} mol^{-1} cm^2 and are typical of uni-univalent electrolytes,[23] indicating that the chloride ligand is tenaciously bound even in this coordinating solvent. In fact, a chloride axial ligand binding constant (eq 2) has been estimated for I, R^1 = *p*-xylylene, R^2 = H, R^3 = CH$_3$, as $K = 2 \times 10^5$ M^{-1}.[14]

$$[FeL(CH_3CN)]^{2+} + Cl^- \overset{K}{\rightleftharpoons} [FeLCl]^+ + CH_3CN \quad (2)$$

(19) "International Tables for X-ray Crystallography"; Kynoch Press: Birmingham, England, 1974; Vol. IV.

(20) DuChamp, D. J. "Program and Abstracts", American Crystallographic Association Meeting, Bozeman, MT, 1964, Paper B14. As modified by Christoph, G. G., at The Ohio State University.

(21) Herron, N.; Grzybowski, J. J.; Matsumoto, N.; Zimmer, L. L.; Christoph, G. G.; Busch, D. H. *J. Am. Chem. Soc.* **1982**, *104*, 1999.

(22) Evans, D. F. *J. Chem. Soc.* **1959**, 2003.

(23) Geary, W. J. *Coord. Chem. Rev.* **1971**, *7*, 81.

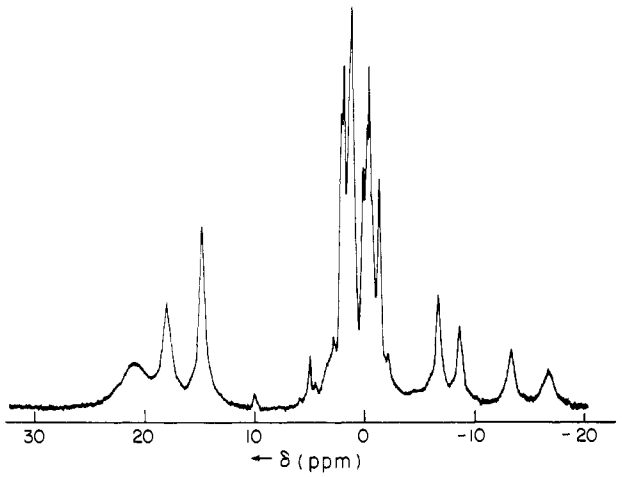

Figure 2. ^1H NMR spectrum of I, $R^1 = (CH_2)_6$, $R^2 = CH_3$, $R^3 = CH_3$, B = Cl, in C^2H_3CN showing paramagnetic shifting and broadening. Shifts are referenced to external Me_4Si.

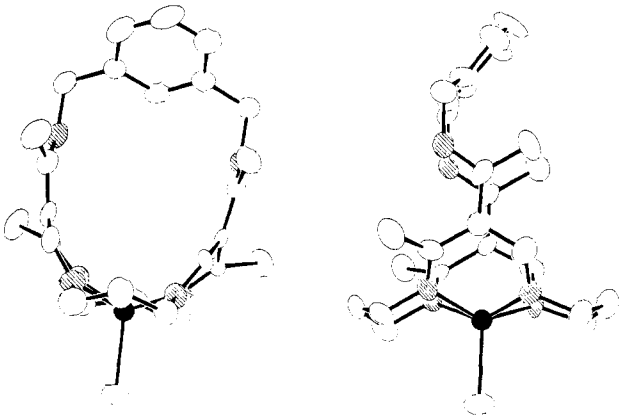

Figure 3. ORTEP drawings showing the side and front view of lacunar complex I, R^1 = *m*-xylylene, R^2 = H, $R^3 = CH_3$, B = Cl. An example of a lid-on isomer.[11] (Fe and N atoms are shaded for clarity.)

Electrochemical data for the complexes I are tabulated in Table IV. The reversible metal(II/III) couple shows a remarkably consistent set of trends, based on the nature of the substituents R^1, R^2, R^3, and B, which allows one to effectively predict the redox potential of any given substitution pattern. The effect of R^1 is very small, covering a range of only some 40 mV for fixed R^2, R^3, and B, and this behavior parallels that previously observed for the analogous nickel(II) complexes. With R^2 = H as a basic value, $R^2 = CH_3$ and $CH_2C_6H_5$ move the potential by −20 to −60 mV and +10 to −20 mV, respectively (R^1, R^3, and B fixed). With $R^3 = CH_3$ as the standard, the potentials are moved by R^3 as follows: C_6H_5, +130 mV; *n*-C_7H_{15}, −20 mV; *p*-$MeOC_6H_4$, +120 mV; *p*-ClC_6H_4, +180 mV; *p*-FC_6H_4, +170 mV (R^1, R^2, and B fixed). Finally, conversion of axial ligand B from Cl to CH_3CN moves the potential some 280 mV more positive as might be anticipated for the replacement of an anionic ligand in the inner coordination sphere. Most of these trends parallel similar behaviors observed for the analogous nickel(II) complexes.[11,12]

^1H NMR spectra of the new iron(II) complexes in C^2H_3CN at room temperature are invariably paramagnetically shifted and broadened as would be predicted on the basis of their solution magnetic moments (Table III). The spectrum generally shows numerous bands in the −50- to +50-ppm range with line widths ranging from 10 to 200 Hz (Figure 2, and see below).

X-ray Crystal Structures. Two crystal structures were completed as described in the experimental section and serve as final confirmation of the proposed structure of these iron(II) complexes as high-spin and five-coordinate. ORTEP drawings of the two complexes are shown in Figures 3 and 4 with their molecular numbering schemes in Figure 5. Bond distances with estimated

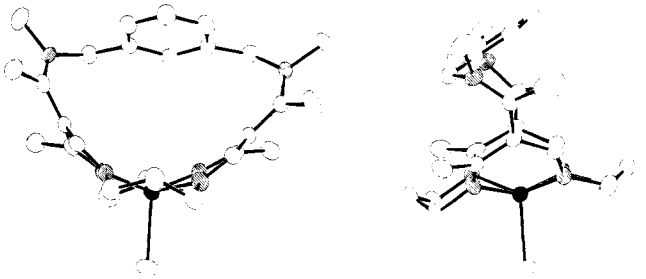

Figure 4. ORTEP drawings showing the side and front view of lacunar complex I, R^1 = *m*-xylylene, $R^2 = CH_3$, $R^3 = CH_3$, B = Cl. An example of a lid-off isomer.[11] (Fe and N atoms are shaded for clarity.)

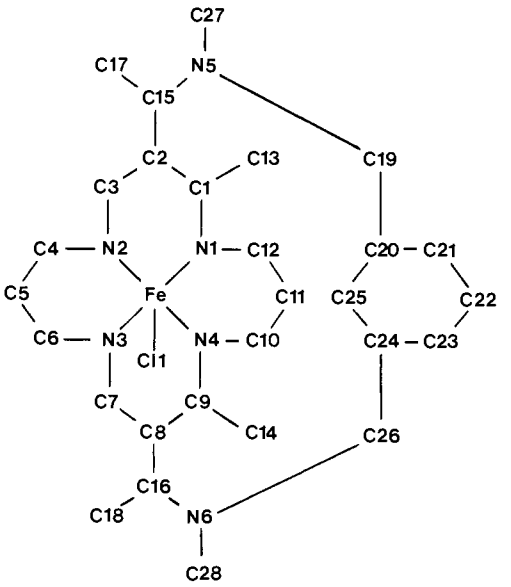

Figure 5. Atom numbering scheme for structures depicted in Figures 3 and 4.

standard derivations (esd's) are listed in Table IIA and bond angles in Table IIB.

It is apparent from the figures that these two complexes have many features in common. Considering first the coordination sphere of the iron(II), it can be seen that the metal ion is five-coordinate in a square-pyramidal geometry with the iron(II) out of the macrocycle N_4 plane toward the axially bound chloride ion. For R^2 = H the displacement is 0.65 Å, and for $R^2 = CH_3$ the displacement is 0.54 Å, this latter distance being very similar to that observed in deoxymyoglobin (0.55 Å).[24,25] The iron–chlorine bond responds to this difference in displacement by lengthening from 2.307, R^2 = H, to 2.326 Å, $R^2 = CH_3$. The average Fe–N distances in both complexes are very similar at 2.114 Å and slightly longer than the 2.08 Å observed for comparable porphyrin complexes.[25] The saturated six-membered chelate rings of the macrocycle are, in both structures, in the chair form since a boat-type conformation would result in unfavorable steric contact with the axial chloride.

The bond distances of the unsaturated portion of the macrocycle and the planar bridge nitrogens N5 and N6 are consistent with extensive delocalization of electron density throughout this portion of the molecules. In both structures, the xylylene ring is suspended over the sixth axial coordination site of the iron(II) providing the cap and much of the rear wall of the apparently rigid cavities. It is apparent from Figures 3 and 4 that the xylylene ring is more directly over the metal if R^2 = H than if $R^2 = CH_3$. This is a consequence of the geometrical isomerism about the bridge nitrogen atoms N5 and N6; when R^2 = H the bridge is *lid on*, and

(24) Collman, J. P. *Acc. Chem. Res.* **1977**, *10*, 265.
(25) Hoard, J. A. In "Porphyrins and Metalloporphyrins"; Smith, K. M., Ed.; Elsevier: New York, 1975; Chapter 8.

Table II. Bond Lengths (Å) and Angles (deg) with Their esd's for Structures I

	a	b		a	b
			A. Lengths		
Fe-Cl	2.307 (3)	2.326 (1)	C10-C11	1.54 (2)	1.503 (7)
Fe-N1	2.131 (8)	2.123 (3)	C11-C12	1.54 (1)	1.522 (8)
Fe-N2	2.079 (7)	2.107 (4)	C15-C17	1.54 (1)	1.498 (8)
Fe-N3	2.074 (7)	2.069 (4)	C15-N5	1.33 (1)	1.352 (6)
Fe-N4	2.163 (7)	2.170 (4)	C16-C18	1.50 (1)	1.504 (8)
N1-C1	1.25 (1)	1.289 (5)	C16-N6	1.32 (1)	1.345 (5)
N1-C12	1.49 (1)	1.472 (8)	C19-N5	1.49 (1)	1.474 (6)
N2-C3	1.28 (1)	1.291 (4)	C19-C20	1.50 (1)	1.518 (6)
N2-C4	1.45 (1)	1.468 (7)	C20-C21	1.39 (1)	1.382 (9)
N3-C6	1.50 (1)	1.486 (7)	C20-C25	1.39 (1)	1.394 (6)
N3-C7	1.31 (1)	1.296 (5)	C21-C22	1.34 (2)	1.384 (7)
N4-C9	1.28 (1)	1.301 (5)	C22-C23	1.39 (2)	1.376 (7)
N4-C10	1.43 (1)	1.464 (8)	C23-C24	1.37 (1)	1.398 (8)
C1-C2	1.52 (1)	1.472 (8)	C24-C25	1.42 (1)	1.383 (6)
C1-C13	1.56 (1)	1.519 (7)	C24-C26	1.51 (1)	1.508 (7)
C2-C3	1.44 (1)	1.429 (7)	C26-N6	1.46 (1)	1.481 (5)
C2-C15	1.43 (1)	1.405 (5)	N5-C27		1.461 (5)
C4-C5	1.50 (1)	1.515 (7)	N6-C28		1.472 (5)
C5-C6	1.52 (1)	1.493 (8)	P-F1		1.575 (4)
C7-C8	1.45 (1)	1.437 (7)	P-F2		1.543 (5)
C8-C9	1.49 (1)	1.461 (8)	P-F3		1.578 (4)
C8-C16	1.41 (1)	1.401 (5)	P-F4		1.500 (4)
C9-C14	1.50 (1)	1.518 (8)	P-F5		1.540 (5)
			P-F6		1.567 (4)
			B. Angles		
N2-Fe-N1	85.1 (3)	84.9 (2)	C15-C2-C1	121.7 (8)	120.3 (4)
N4-Fe-N1	83.5 (3)	87.4 (1)	C15-C2-C3	117.9 (8)	118.2 (5)
N3-Fe-N2	86.8 (3)	89.3 (2)	C2-C3-N2	127.1 (8)	126.8 (5)
N4-Fe-N3	83.6 (3)	84.1 (2)	C5-C4-N2	113.6 (8)	113.2 (4)
C1-N1-Fe	128.7 (8)	129.4 (4)	C6-C5-C4	117.7 (9)	116.6 (5)
C12-N1-Fe	111.3 (8)	110.1 (2)	C5-C6-N3	112.0 (9)	112.7 (3)
C12-N1-C1	119.9 (9)	120.2 (4)	C8-C7-N3	124.9 (8)	127.7 (5)
C3-N2-Fe	120.2 (6)	124.4 (4)	C9-C8-C7	121.3 (7)	120.8 (4)
C4-N2-Fe	118.3 (6)	118.5 (2)	C16-C8-C7	116.0 (8)	116.1 (5)
C4-N2-C3	117.3 (7)	116.2 (4)	C16-C8-C9	122.4 (9)	122.3 (4)
C6-N3-Fe	116.5 (6)	116.9 (3)	C8-C9-N4	118.3 (8)	121.5 (5)
C7-N3-Fe	123.9 (7)	126.7 (3)	C14-C9-N4	124.1 (8)	120.8 (5)
C7-N3-C6	116.8 (8)	115.2 (4)	C14-C9-C8	117.1 (8)	117.2 (4)
C9-N4-Fe	129.1 (7)	129.5 (4)	C11-C10-N4	113.3 (8)	113.8 (4)
C10-N4-Fe	111.0 (5)	109.4 (3)	C12-C11-C10	116.5 (9)	115.4 (5)
C10-N4-C9	119.8 (8)	119.6 (4)	C11-C12-N1	108.5 (8)	110.1 (4)
C2-C1-N1	118.3 (9)	120.6 (4)	C17-C15-N5	116.5 (8)	116.5 (3)
C13-C1-N1	125.2 (8)	122.2 (5)	C17-C15-C2	122.9 (8)	124.1 (4)
C13-C1-C2	116.2 (8)	116.7 (4)	N5-C15-C2	120.5 (8)	119.3 (5)
C3-C2-C1	120.2 (7)	121.4 (3)	C18-C16-N6	117.0 (7)	115.1
C18-C16-C8	123.1 (8)	122.9 (4)	C21-C20-C25	118.2 (9)	118.6 (4)
N6-C16-C8	119.9 (8)	122.0 (4)	C25-C20-C19	121.5 (8)	117.7 (5)
C19-N5-C15	124.4 (7)	121.0 (3)	C22-C21-C20	119.9 (9)	120.3 (5)
C27-N5-C15		122.5 (4)	C28-C22-C21	122.4 (10)	121.1 (6)
C27-N5-C19		115.5 (4)	C24-C23-C22	120.2 (9)	119.4 (4)
C26-N6-C16	125.3 (8)	122.7 (3)	C25-C24-C23	117.2 (9)	119.2 (4)
C28-N6-C16		121.7 (3)	C26-C24-C23	121.9 (9)	122.1 (4)
C28-N6-C26		115.2 (3)	C26-C24-C25	120.7 (8)	118.4 (5)
C20-C19-N5	111.0 (8)	113.7 (5)	C24-C25-C20	122.0 (9)	119.2 (4)
C21-C20-C19	120.3 (9)	123.6 (4)	C24-C27-N6	112.5 (7)	114.7 (5)

[a] R^1 = *m*-xylylene, R^2 = H, R^3 = CH_3. [b] R^1 = *m*-xylylene, R^2 = CH_3, R^3 = CH_3.

with R^2 = CH_3 it is *lid off*.[11,14] This isomerism dramatically affects the size and shape of the resultant cavities. The lid-on structure (Figure 3) has the bridge rising almost perpendicularly to the macrocycle N_4 plane, resulting in a tall narrow lacuna. In the lid-off structure (Figure 4) the bridge lies almost parallel to the macrocycle N_4 plane, yielding a shorter, wider cavity. The lacuna dimensions vary tremendously between the two structures as a consequence of this isomerism, when R^2 = H the complex is 7.6 Å tall in the front (to C22) and 5.5 Å tall in the rear (to C25) while R^2 = CH_3 has corresponding dimensions 5.0 and 3.9 Å (distances measured perpendicularly from the N_4 plane to the center of the indicated carbon atom). The cavity widths between N5 and N6 are 5.0 (R^2 = H) and 7.3 Å(R^2 = CH_3). When the van der Waals radii are taken into account the maximum lacuna height and width are 4.2 and 2.1 Å (R^2 = H) and 1.7 and 4.3 Å (R^2 = CH_3). The dihedral angles between the xylylene rings and the macrocycle N_4 plane are 53° (R^2 = H) and 30° (R^2 = CH_3).[26]

One further feature of the complex with R^2 = H is the extensive hydrogen bonding within the lattice (Figure 6). Although H atoms were not located in this structure determination, the distances between non-hydrogen atoms clearly show the extent of interaction. The counterion chloride is 3.3 Å from one bridge nitrogen atom and 3.0 Å from one methanol oxygen atom. The coordinated chloride is 3.6 Å from the second methanol oxygen atom, and the two methanol oxygen atoms are 3.35 Å from each other. All of these distances are well within normal H-bonding

(26) The variation in cavity dimensions with structural parameters and the chemical consequences thereof have been discussed in ref 13, 14, and 27.

(27) Stevens, J. C.; Jackson, P. C.; Schammel, W. P.; Christoph, G. G.; Busch, D. H. *J. Am. Chem. Soc.* **1980**, *102*, 3283.

Table III. Magnetic Moments of the New Iron(II) Complexes of Lacunar Ligands I

R^1	R^2	R^3	solid (298 K)	acetonitrile soln (301.6 K)	311APW[a] soln (301 K)
m-xylylene	H	CH_3	5.18	4.97	5.26
m-xylylene	CH_3	CH_3	5.38	5.09	5.11
m-xylylene	CH_3	C_6H_5		5.12	5.17
m-xylylene	$CH_2C_6H_5$	CH_3		5.04	5.20
m-xylylene	$CH_2C_6H_5$	C_6H_5		4.99	5.11
m-xylylene	CH_3	C_7H_{15}		5.64	5.55
m-xylylene	CH_3	*p*-$MeOC_6H_4$		5.00	4.97
m-xylylene	CH_3	*p*-ClC_6H_4		5.11	5.08
m-xylylene	CH_3	*p*-FC_6H_4		5.24	5.20
$(CH_2)_4$	H	CH_3	4.99	4.91	4.99
$(CH_2)_4$	CH_3	CH_3		4.95	4.95
$(CH_2)_4$	CH_3	C_6H_5		4.96	5.04
$(CH_2)_5$	H	CH_3		5.02	4.88
$(CH_2)_5$	CH_3	CH_3		5.00	5.11
$(CH_2)_5$	CH_3	C_6H_5		4.90	4.99
$(CH_2)_6$	H	CH_3	5.35	5.08	5.05
$(CH_2)_6$	CH_3	CH_3	4.90	5.27	5.25
$(CH_2)_6$	CH_3	C_6H_5		5.16	5.17
p-xylylene	H	CH_3		5.20	5.21
7-fluorenylidene	H	CH_3		5.01	4.97

[a] 3:1:1 by volume mixture of acetone/pyridine/water.

Table IV. Electrochemical Data for the First Oxidation Process of Iron(II) Complexes I[a]

R^1	R^2	R^3	B	$E_{1/2}$, V	E_{pox}, V	E_{pred}, V	$\lvert E_{3/4} - E_{1/4} \rvert$, mV
m-xylylene	H	CH_3	Cl	−0.34	−0.30	−0.38	60
m-xylylene	CH_3	CH_3	Cl	−0.40	−0.37	−0.43	60
m-xylylene	CH_3	C_6H_5	CH_3CN	+0.02	+0.05	−0.02	60
m-xylylene	$CH_2C_6H_5$	CH_3	CH_3CN	−0.06	−0.03	−0.10	60
m-xylylene	$CH_2C_6H_5$	C_6H_5	CH_3CN	+0.06	+0.10	~+0.03	70
m-xylylene	CH_3	CH_3	CH_3CN	−0.12	−0.09	−0.15	60
m-xylylene	CH_3	*p*-$MeOC_6H_4$	Cl	−0.28	−0.25	−0.32	70
m-xylylene	CH_3	*p*-ClC_6H_4	Cl	−0.22	−0.18	−0.25	70
m-xylylene	CH_3	*p*-FC_6H_4	Cl	−0.23	−0.18	−0.27	70
m-xylylene	CH_3	C_7H_{15}	Cl	−0.42	−0.33	−0.42	70
$(CH_2)_4$	H	CH_3	Cl	−0.39	−0.35	−0.41	60
$(CH_2)_4$	CH_3	CH_3	Cl	−0.43	−0.40	−0.47	60
$(CH_2)_4$	CH_3	C_6H_5	Cl	−0.29	−0.26	−0.32	60
$(CH_2)_5$	H	CH_3	Cl	−0.41	−0.37	−0.46	80
$(CH_2)_5$	CH_3	CH_3	Cl	−0.44	−0.41	−0.48	60
$(CH_2)_5$	CH_3	C_6H_5	Cl	−0.31	−0.27	−0.35	60
$(CH_2)_6$	H	CH_3	Cl	−0.38	−0.32	−0.42	90
$(CH_2)_6$	CH_3	CH_3	Cl	−0.40	−0.36	−0.44	70
$(CH_2)_6$	CH_3	C_6H_5	Cl	−0.27	−0.24	−0.31	60
$(CH_2)_6$	$CH_2C_6H_5$	C_6H_5	Cl	−0.24	−0.20	−0.27	80
7-fluorenylidene	H	CH_3	Cl	−0.38	−0.34	−0.42	70

[a] In acetonitrile containing 0.1 M *n*-Bu_4NBF_4 supporting electrolyte, $Ag/AgNO_3$ (0.1 M) reference electrode, Pt-disc electrode, 0.05 V s^{-1} scan rate. T = 22 °C under N_2.

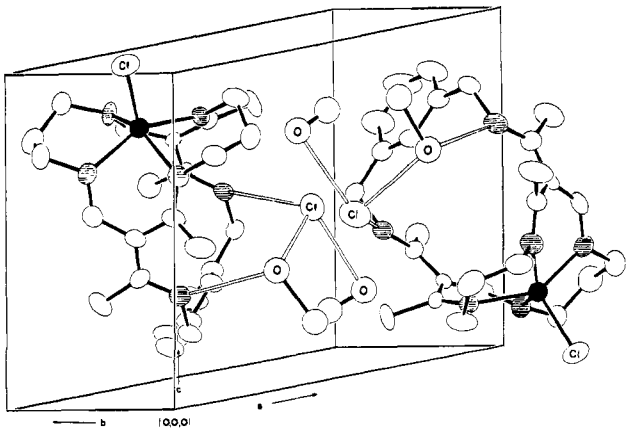

Figure 6. Crystal packing diagram of I, R^1 = *m*-xylylene, R^2 = H, R^3 = CH_3, B = Cl, showing hydrogen-bonded atoms (open bonds). (Fe and N atoms are shaded for clarity.)

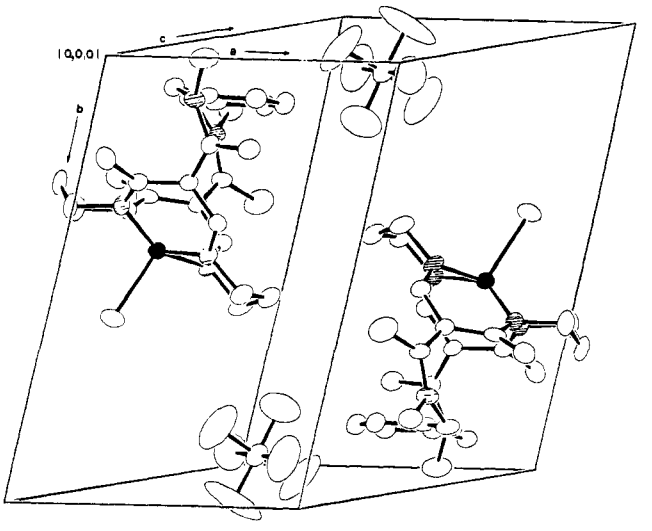

Figure 7. Crystal packing diagram of I, R^1 = *m*-xylylene, R^2 = CH_3, R^3 = CH_3, B = Cl. (Fe and N atoms are shaded for clarity.)

limits for the atoms involved. Crystal packing diagrams for both complexes are shown in Figures 6 and 7.

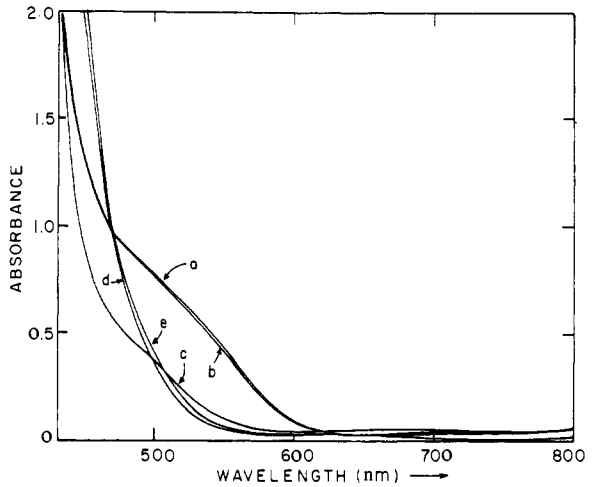

Figure 8. Visible spectra of I, R^1 = *m*-xylylene, $R^2 = CH_3$, $R^3 = CH_3$, B = Cl, in various solvents [Fe] = 5.6×10^{-4} M: (a) acetone, (b) 4:1 by volume acetone/pyridine, (c) 4:1 by volume acetone/water, (d) 3:1:1 by volume acetone/pyridine/water. (e) I, R^1 = *m*-xylylene, $R^2 = CH_3$, $R^3 = CH_3$, B = CH_3CN. [Fe] = 5.6×10^{-4} M in 4:1 by volume acetone/pyridine.

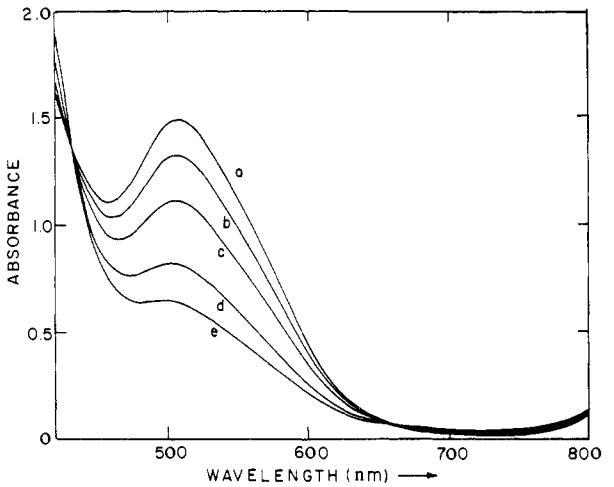

Figure 9. Visible spectra of I, $R^1 = (CH_2)_6$, $R^2 = CH_3$, $R^3 = C_6H_5$, B = Cl, in 3:1:1 acetone/pyridine/water at (a) 234.6 K, (b) 239.3 K, (c) 245.7 K, (d) 254.5 K, and (e) 260.9 K.

Axial Ligand Equilibria in Solution. As indicated above, the lacunar iron(II) complexes described tend to be five-coordinate in the solid state and appear to remain so upon dissolution in simple solvents. However, their axial ligand behavior falls into two distinct classes. First, the bis(hexafluorophosphate) salts, which presumably have acetonitrile as their fifth ligand (elemental analyses, Table I), dissolve in acetonitrile to give the expected five-coordinate complexes which may have their axial acetonitrile ligand readily displaced by another nitrogenous base such as pyridine or 1-methylimidazole. This is shown by electrochemical data; $E_{1/2}$ for the Fe(II/III) couple becomes more negative when these bases are added while the visible spectra give no evidence of formation of six-coordinate bis(base) species. Also, their magnetic moments and ^1H NMR spectra in a variety of solvents indicate that the complexes remain five-coordinate.

On the other hand, the chlorohexafluorophosphate salts appear to have chloride tenaciously bound as the fifth axial ligand both in the solid state and in anhydrous solution. Both crystal structures, above, indicate that this is so while the molar conductivities of such species indicate that they are uni-univalent electrolytes in solution. As noted above, an estimate value for the chloride binding constant (eq 2) is surprisingly large at $K = 2 \times 10^5$ M^{-1} in acetonitrile.[14] Furthermore, the half-wave potentials of these complexes in CH_3CN are essentially unaffected by the addition of large excesses of such axial nitrogenous bases as pyridine or 1-methylimidazole, indicating (a) that the chloride is not easily displaced by such ligands, and (b) that the cavities of these complexes are sufficiently demanding to prevent access of these nitrogenous bases to the sixth coordination site of the iron(II). This latter point was confirmed by visible spectral studies on such anhydrous solutions where no evidence for low-spin six-coordinate species was detected. The unusual persistence of chloride as the axial ligand was particularly undesirable since any attempts to produce dioxygen carriers of these iron complexes would be expected to find major success only with a nitrogenous base as the axial ligand.[28,29] A way to easily and completely replace chloride by base was therefore sought, and a simple solution quickly became apparent. The addition of as little as 5% water to an acetone solution of the complex containing 20% of the desired nitrogenous base effects the desired transformation. Figure 8 details this process. The visible spectrum of I, R^1 = *m*-xylylene, $R^2 = CH_3$, $R^3 = CH_3$, B = Cl, in acetone is essentially featureless except for a small shoulder on the intense charge-transfer band at ~520 nm. Addition of the 20% pyridine leaves the spectrum quantitatively unchanged while addition of 20% water causes a dramatic decrease in the aforementioned shoulder. Addition of both 20% pyridine *and* 20% water results in a spectrum with absolutely no shoulder in the visible region. Comparing this spectrum with one of I, R^1 = *m*-xylylene, $R^2 = CH_3$, $R^3 = CH_3$, B = CH_3CN, prepared by an independent route[14] in acetone containing 20% pyridine, i.e., B = pyridine, based on electrochemical measurements (vide supra) produces a quantitative match. Addition of 20% water *and* 20% pyridine fails to change the spectrum further. These results are best interpreted as indicating that the chloride axial ligand is quantitatively replaced by pyridine in a solvent system consisting of 60% acetone, 20% pyridine, and 20% water (by volume), hereafter abbreviated to 311APW. Similar findings were noted with 1-methylimidazole as the axial base and for other lacunar complexes.

In this mixed solvent system the complexes do indeed lose their axial chloride, probably as a consequence of its hydration by the water component,[30] but they appear to remain five-coordinate and high spin at room temperature as judged by their visible spectra and magnetic moments. This was a little surprising at first since this solvent contains a high concentration of hydroxide ion (pH ≃10), which is both small enough and sufficiently nucleophilic that one might expect it to enter the lacuna and force the metal ion to become six-coordinate. For most of the complexes this is not the case and is probably a consequence of the thermodynamically expensive procedure of removing OH^- from a water solvation sheath and placing it into the hydrophobic environment of the lacuna.

One set of complexes does not follow this pattern of behavior, however. The complexes with $R^1 = (CH_2)_6$ appear to involve an equilibrium between a five- and a six-coordinate geometry with the higher coordination number being favored at lower temperatures. Visible spectral changes accompanying temperature changes are exemplified in Figure 9 for $R^1 = (CH_2)_6$, $R^2 = CH_3$, and $R^3 = C_6H_5$, and the growth of the band at 508 nm is accompanied by sharp isosbestic points at 663 and 432 nm as the temperature is lowered, both of which indicate a simple five- to six-coordinate geometry change. The band at 508 nm is very reminiscent of the $M \rightarrow \pi^*$ transition of low-spin six-coordinate (hexaimine)iron(II) tris(bpy) or tris(phen) complexes.[31] That the apparent coordination number change is accompanied by a spin change is confirmed by the variable-temperature magnetic moment for $R^1 = (CH_2)_6$, $R^2 = CH_3$, and $R^3 = C_6H_5$, which falls from 5.17 μ_B at 301.6 K to 4.51 μ_B at 237 K,[32] the latter value

(28) Traylor, T. G.; Traylor, P. S. *Ann. Rev. Biophys. Bioeng.* **1982**, *11*, 105.
(29) Jones, R. D.; Summerville, D. A.; Basolo, F. *Chem. Rev.* **1979**, *79*, 139.
(30) Doeff, M. M.; Sweigart, D. A. *Inorg. Chem.* **1982**, *21*, 3699.
(31) Krumholtz, P. *J. Am. Chem. Soc.* **1953**, *75*, 2163.

corresponding to approximately 24% of low-spin material. This coordination number equilibrium has only been observed for the $R^1 = (CH_2)_6$ bridged derivatives, and it is believed to be a consequence of the water or hydroxide in the solvent since the phenomenon occurs only in partially aqueous media. In 4/1 acetone/pyridine the complexes remain high spin and five-coordinate. This implies that the $(CH_2)_6$ bridge is sufficiently open to allow a small sixth ligand to enter the lacuna or to enter the lacuna *and* remain solvated to water in solution making its coordination thermodynamically favorable.

Interaction with Dioxygen. Although initial studies showed discouragingly rapid irreversible reactions between examples of these iron(II) complexes and dioxygen, studies with the analogous cobalt(II), O_2[16] and iron(II) CO[14] systems provided the basis for selecting structural modifications that do produce the desired reversible process. The most revealing result is the exceptionally large dioxygen affinities that the cobalt(II) complexes display. In general,[28] iron(II) species interact with O_2 some 100 to 1000 times more strongly than do the corresponding cobalt(II) species. Since the lacunar cobalt complexes have, by far, the greatest O_2 affinities known among the Pauling type $Co-O_2$ adducts, the corresponding iron(II) complexes should have phenomenal O_2 affinities. It is also true that iron serves to activate O_2 in many heme proteins,[33] and it might be anticipated that the reactivity of O_2 bound to Fe would increase along with an increase in the O_2 affinity of the iron complex. Consequently, lacunar ligands having structural parameters that weaken the O_2 affinity of the cobalt(II) complex are expected to give reversible O_2 binding to iron(II). On this basis the complex I, R^1 = *m*-xylylene, $R^2 = CH_3$, and $R^3 = CH_3$, was chosen for detailed study, and the positive results were reported in a preliminary communication.[34] The crystal structure of the complex is shown in Figure 4, and as its cobalt(II) complex the binding constant for O_2 is 0.0019 ± 0.0001 $torr^{-1}$ at −41.5 °C in 3:1:1 by volume acetone/water/1-methylimidazole.

The iron(II) complex proved to be a moderately successful O_2 carrier as reported earlier[34] with a binding constant some 1000 times greater than its cobalt(II) analogue. The problem with the complex, however, was that fully reversible O_2 binding was only observed at temperatures below −35 °C, while at higher temperatures irreversible oxidation to iron(III) also occurs. In order to improve this situation, a detailed study of the autoxidation process was carried out and the important results for present purposes may be summarized in eq 3 or 4.

$$Fe^{II}LB + O_2 \underset{}{\overset{K_{O_2}}{\rightleftharpoons}} Fe^{II}LBO_2 \xrightarrow[RDS]{k} Fe^{III}LB + O_2^- \quad (3)$$

$$Fe^{III}LB + O_2^- \xleftarrow[RDS]{+O_2 k} FeLB + O_2 \overset{K_{O_2}}{\rightleftharpoons} Fe^{II}LBO_2 \quad (4)$$

The kinetics of autoxidation are first order in iron concentration while displaying a complex oxygen dependence consistent with the prior equilibrium formation of the dioxygen adduct. This data allows both eq 3 and 4 to be consistent as mechanisms but does not allow a distinction between them. However, both schemes involve a charge transfer from iron to dioxygen and production of iron(III) and superoxide species. These charge separation processes ought to be favored by the presence of protons or polar solvent molecules in the vicinity of the active site.[24,29] One might anticipate, therefore, that the presence of bulky hydrophobic substituents around the active site might hinder this autoxidation pathway. In addition, the redox potential of the iron center should affect these charge transfer processes, and any alteration in substituents R^2 and R^3 that shifts the potential toward more positive values should retard the autoxidation reaction.

With these two concepts in mind, a series of other substituted iron(II) complexes was synthesized, and the O_2 carrying abilities

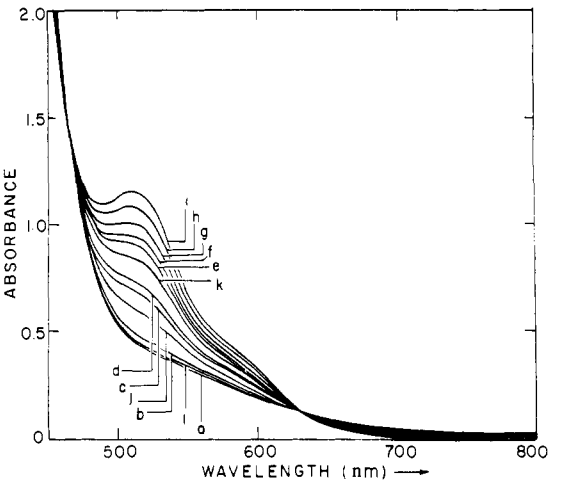

Figure 10. Visible spectral changes accompanying exposure of I, R^1 = *m*-xylylene, $R^2 = CH_2C_6H_5$, $R^3 = C_6H_5$, B = CH_3CN, to various partial pressures of dioxygen. Solvent: 4:1 by volume toluene/1-methylimidazole at 0.0 °C. P_{O_2} (torr), in order of recording: (a) 0, (b) 1.9, (c) 22, (d) 38, (e) 67, (f) 99, (g) 150, (h) 300, (i) 760, (j) 12, (k) 50, (l) 0. Exposure to O_2 was for 200 s, plot time was 250 s.

of the new compounds were explored. In all instances, the iron complexes dissolve to give a featureless visible spectrum, which, upon exposure to dioxygen, displays similar characteristic spectral changes. A strong band grows in around 520 nm with a shoulder around 620 nm (Figure 10). These features increase in intensity as the partial pressure of O_2 is increased, often with isosbestic points similar to those shown in Figure 10. The spectral changes may be more or less quantitatively reversed by flushing the solution with pure N_2. Within this generalized behavior there are extremes of reversibility as described in Table V. When R^1 is a simple polymethylene chain, the behavior toward dioxygen varies widely with respect to reversibility, K_{O_2}, and stability toward autoxidation. The $(CH_2)_4$ bridged complex autoxidizes very rapidly in 311APW even at −40 °C, and this is believed to be a consequence of the poor steric protecting ability of the tetramethylene bridge. The $(CH_2)_5$ and $(CH_2)_6$ bridged materials also autoxidize, but not so rapidly. They have extremely large K_{O_2}'s depending on the nature of B, and the K_{O_2} appears to rise dramatically in changing from $(CH_2)_5$ to $(CH_2)_6$ as was anticipated from the earlier data with the Co^{II} complexes. When B = py for $R^1 = (CH_2)_5$ and when B = Cl for $R^1 = (CH_2)_6$ the value is too large to measure with our apparatus and the lower limit is quoted in Table V. Clearly the limited data available for the polymethylene chain complexes show (a) that the O_2 behavior of the lacunar complexes is not limited to *m*-xylylene bridges and (b) that K_{O_2} can be dramatically affected by the nature of R^1 and B over an enormous range as was observed for the equivalent cobalt(II) complexes.[16] The mechanism of autoxidation of iron(II) dioxygen carriers is the subject of ongoing studies, and the autoxidation in partially aqueous solvents is interpreted as arising from the poor steric protection offered by polymethylene bridges.

Most of our synthetic work, therefore, has been carried out by using the R^1 = *m*-xylylene bridged materials in Table V. Certain of these data appeared in previous communications,[34,35] but the complete set, to date, is presented here. A number of interesting points are worth noting: (i) When R^2 = H the iron(II) complexes of *m*-xylylene or any R^1 bridge have been found to autoxidize very rapidly, even at the lowest temperatures we routinely use (233 K). This behavior has been attributed either to the R^2 proton attracting water to the cavity by hydrogen bonding or to the R^2 proton being acidic and therefore capable of protonating the bound dioxygen. The juxtaposition of the R^2 substituent and the bound O_2 ought to make this latter process very facile, and the resultant elimination of reduced O_2 as hydroperoxyl radical may thus be

(32) The temperature profile of μ_{eff} is as follows: 301 K, 5.17 μ_B; 265 K, 5.10 μ_B; 256 K, 5.04 μ_B; 244 K, 4.85 μ_B; 237 K, 4.51 μ_B.

(33) White, R. E.; Coon, M. J. *Ann. Rev. Biochem.* **1980**, *49*, 315.
(34) Herron, N.; Busch, D. H. *J. Am. Chem. Soc.* **1981**, *103*, 1236.
(35) Herron, N.; Cameron, J. H.; Neer, G. L.; Busch, D. H. *J. Am. Chem. Soc.* **1983**, *105*, 298.

Table V. Behavior of Iron(II) Lacunar Complexes I with Dioxygen

R^1	R^2	R^3	B	K_{O_2}, $torr^{-1}$ (temperature of estimate, K)[a]	solvent
m-xylylene	CH_3	CH_3	py	0.16 ± 0.01 (231.5)	311APW
m-xylylene	CH_3	CH_3	py	0.08 ± 0.01 (231.5)	4/1 Ace/py
m-xylylene	CH_3	CH_3	Cl	0.015 ± 0.003 (231.5)	4/1 Ace/py
m-xylylene	CH_3	CH_3	1-Mim	1.7 ± 0.2 (231.5)	4/1 Ace/Mim
m-xylylene	H	CH_3	Cl	irreversible (231.5)	311APW
m-xylylene	$CH_2C_6H_5$	CH_3	py	0.016 ± 0.002 (238.3), 0.0133 ± 0.002 (239), 0.0088 ± 0.0012 (243) 0.0057 ± 0.0011 (246.5), 0.005 ± 0.001 (246) 0.0030 ± 0.0008 (253.5)	311APW
m-xylylene	CH_3	n-C_7H_{15}	py	0.120 ± 0.004 (253)	311APW
m-xylylene	CH_3	C_6H_5	py	0.125 ± 0.004 (232.5), 0.119 ± 0.004 (233.8) 0.032 ± 0.002 (243), 0.025 ± 0.002 (243.9) 0.0112 ± 0.008 (253), 0.0045 ± 0.0003 (261)	311APW
m-xylylene	CH_3	C_6H_5	1-Mim	0.0067 ± 0.0005 (273)	4/1 toluene/Mim
m-xylylene	CH_3	C_6H_5	1-Mim	0.0053 ± 0.0002 (273)	4/1 acetonitrile/Mim
m-xylylene	$CH_2C_6H_5$	C_6H_5	py	0.55 ± 0.07 (235.3), 0.20 ± 0.01 (240.7) 0.050 ± 0.001 (251.7), 0.0091 ± 0.002 (262.9) 0.0095 ± 0.003 (262.8), 0.0025 ± 0.0004 (273)	311APW
m-xylylene	$CH_2C_6H_5$	C_6H_5	1-Mim	0.022 ± 0.001 (273)	4/1 toluene/Mim
m-xylylene	$CH_2C_6H_5$	C_6H_5	1-Mim	0.016 ± 0.001 (273)	4/1 acetonitrile/Mim
m-xylylene	$CH_2C_6H_5$	C_6H_5	1-Mim	0.031 ± 0.003 (273)	4/1 water/Mim
m-xylylene	$CH_2C_6H_5$	C_6H_5	1-Mim	0.041 ± 0.0003 (273)	4/1 methanol/Mim
m-xylylene	$CH_2C_6H_5$	C_6H_5	1-Mim	0.0086 ± 0.0007 (273)	4/1 acetone/Mim
m-xylylene	$CH_2C_6H_5$	C_6H_5	1-Mim	0.021 ± 0.001 (273), 0.0012 ± 0.0003 (293)	Mim
m-xylylene	CH_3	*p*-$MeOC_6H_4$	py	0.0325 ± 0.0009 (231.9), 0.013 ± 0.0005 (238.8) 0.0065 ± 0.0003 (243.5), 0.0046 ± 0.0004 (241) 0.0030 ± 0.0001 (249.2), 0.0014 ± 0.0001 (257.3) 0.00089 ± 0.00007 (263.2)	311APW
m-xylylene	CH_3	*p*-ClC_6H_4	py	0.076 ± 0.004 (238.5), 0.034 ± 0.002 (243.2) 0.0073 ± 0.0005 (253.9), 0.0022 ± 0.0001 (263.6)	311APW
m-xylylene	CH_3	*p*-FC_6H_4	py	0.026 ± 0.002 (243.2), 0.0101 ± 0.0003 (250) 0.0037 ± 0.0001 (257.6), 0.00125 ± 0.0001 (266.4)	311APW
$(CH_2)_4$	CH_3	CH_3	Cl	irreversible (233)	311APW
$(CH_2)_5$	CH_3	C_6H_5	Cl	0.03 ± 0.005 (254)	acetone
$(CH_2)_5$	CH_3	C_6H_5	py	>100 (242)	311APW
$(CH_2)_5$	CH_3	C_6H_5	Cl	0.01 ± 0.002 (273)	pyridine
$(CH_2)_6$	CH_3	CH_3	Cl	>200 (233)	acetone

[a] K_{O_2} defined by $FeLB + O_2 \overset{K_{O_2}}{\rightleftharpoons} FeLBO_2$. When a number is quoted it means that a K_{O_2} was measurable at the temperature given and that during the experiment to estimate K_{O_2} irreversible autoxidation reactions were negligible as judged by the visible spectra.

considerably enhanced. (ii) The effect of the axial base B is as anticipated,[28,29] aromatic nitrogeneous bases giving larger K_{O_2}'s than chloride and the more basic 1-methylimidazole giving larger K_{O_2}'s than pyridine for any given iron(II) complex. (iii) The effect of solvent on K_{O_2} is a little less clear; a wide range of solvents has been studied for the complex I, R^1 = *m*-xylylene, $R^2 = CH_2C_6H_5$, $R^3 = C_6H_5$, B = 1-Mim, at 273 K. As expected, water as the bulk solvent gives the highest K_{O_2} in accord with earlier observations,[28,29] but the ordering of the rest of the solvents in decreasing order of K_{O_2}, toluene ≃ 1-methylimidazole > acetonitrile > acetone > methanol, shows no obvious trend either of solvent polarity or hydrophobicity and perhaps reflects (a) degree of ion pairing in the particular solvent system or (b) relative solubility of dioxygen in each solvent, which is not accounted for in our method of estimating K_{O_2} at a standard state of 1 torr. Alternatively, the data may indicate that the FeO_2 unit is best viewed not as a charge-separated $Fe^{III}O_2^-$ species[29] but rather as an iron(II) oxygenyl unit with very little charge separation.[36] (iv) By contrast, the effect of increasing steric bulk and/or electronic effects on the stability toward autoxidation of these iron complexes is very clear. Just looking at the highest temperature at which a K_{O_2} value may be estimated for the R^1 = *m*-xylylene series shows that as the steric bulk of substituents R^2 and R^3 increases, so does the autoxidation stability.[35] Likewise, as the metal(II/III) redox couple moves more positive (Table IV) the autoxidation stability increases also. The stability of the complex I, R^1 = *m*-xylylene, R^2 = benzyl, R^3 = phenyl, is quite remarkable. The X-ray crystal structure of the nickel(II) complex of this ligand has been reported,[12] and a space-filling representation of the structure is shown in Figure 11. The structure illustrates the highly sterically protected environment provided for dioxygen within the lacuna of this structure. In aqueous solution the Fe(II) complex of this ligand is reversible in its interaction with dioxygen at temperatures as high as 273 K, but even more remarkable is its behavior in nonaqueous solvents. In such solvents the complex binds oxygen reversibly with little evidence for autoxidation even at 295 K (Figure 12) over a period of a few hours of continuous oxygenation/deoxygenation cycles. This complex represents, therefore, by far the finest example of a totally synthetic non-porphyrin iron(II) dioxygen carrier in terms of autoxidation stability and, indeed, rivals even the better examples from the porphyrin realm.[24,29]

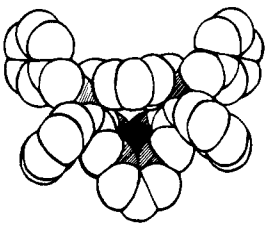

Figure 11. Space-filling representation of the X-ray structure of the nickel(II) complex I, R^1 = *m*-xylylene, $R^2 = CH_2C_6H_5$, $R^3 = C_6H_5$, as viewed into the lacuna. (Ni and N atoms are shaded for clarity.[12])

It has been possible to measure K_{O_2} at different temperatures for a number of the R^1 = *m*-xylylene complexes (Table V) and this, in turn, permitted Van't Hoff plots and the estimation of the thermodynamic parameters for dioxygen binding. These are reported in Table VI. The values are fairly unremarkable except for the near constancy of the value of ΔS at ~−75 eu. Our

(36) Caughey, W. S.; Choc, M. G.; Houtchens, R. A. "Biochemical and Clinical Aspects of Oxygen"; Academic Press: New York, 1979; p 1.

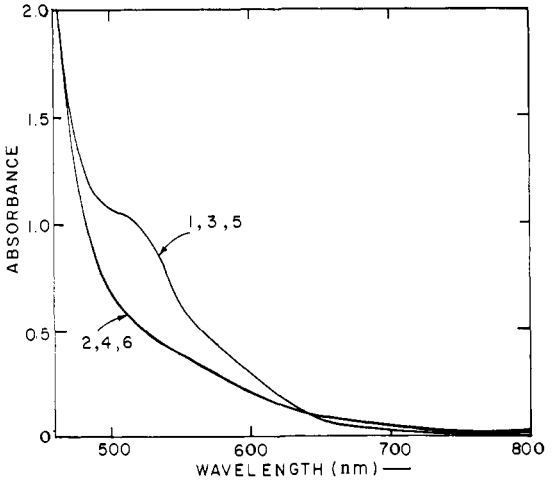

Figure 12. Visible spectra of I, R^1 = *m*-xylylene, $R^2 = CH_2C_6H_5$, $R^3 = C_6H_5$, B = CH_3CN, 2.5×10^{-3} M in 4:1 by volume CH_3CN/1-methylimidazole at 295 K. Plots show three oxygenation (no. 1, 3, and 5) and deoxygenation (no. 2, 4, and 6) cycles of the complex with 748 torr O_2 for 200 s and 748 torr N_2 for 200 s waiting 20 min between oxygenation and deoxygenation. Total time of experiment, ~90 min.

Table VI. Thermodynamic Parameters[a] of Dioxygen Binding to Iron(II) Lacunar Complexes I in 311APW

R^1	R^2	R^3	ΔH, kcal mol^{-1}	ΔS, cal deg^{-1} mol^{-1}	R^b
m-xylylene	$CH_2C_6H_5$	CH_3	−12.9 ± 0.6	−63 ± 2	0.9970
m-xylylene	CH_3	C_6H_5	−14.2 ± 0.5	−65 ± 2	0.9973
m-xylylene	$CH_2C_6H_5$	C_6H_5	−17.5 ± 0.4	−76 ± 2	0.9991
m-xylylene	CH_3	*p*-$MeOC_6H_4$	−15.9 ± 0.6	−75 ± 3	0.9917
m-xylylene	CH_3	*p*-ClC_6H_4	−17.6 ± 0.6	−76 ± 3	0.9995
m-xylylene	CH_3	*p*-FC_6H_4	−16.8 ± 0.5	−76 ± 2	0.9997

[a] Standard state of 1 torr. [b] Linear least-squares correlation coefficient of Van t'Hoff plot.

previous reports on cobalt(II) dioxygen carriers of these lacunar ligands consistently reported values of ΔS as −65 eu, which corresponds rather closely with the removal of all translational and rotational degrees of freedom from gaseous dioxygen.[37] The somewhat more negative numbers reported here for the iron complexes imply that not only are the degrees of freedom removed from the O_2 upon coordination but also that either the solvent or ligand itself undergo some ordering as O_2 binds. This may be related to the movement of iron(II) into the N_4 macrocycle plane as O_2 binds (Figures 3 and 4 show the Fe(II) displacement in the deoxy complexes), causing a reordering of the ligand superstructure.

The dioxygen adducts of these lacunar complexes have yet to yield single crystals for X-ray analysis, but several other supporting techniques have confirmed the presence of a 1:1 dioxygen adduct. Gas uptake measurements have shown that 1.0 ± 0.2 mol of O_2 is absorbed per mol of Fe(II). The resultant adduct is EPR silent and in fact is diamagnetic as judged by ^{1}H NMR spectra (Figure 13) and Evans magnetic moment measurements. The ^{1}H NMR spectrum of the unoxygenated complex is clearly paramagnetically shifted and broadened, consistent with its high-spin configuration (Table III), but upon exposure to pure O_2 under conditions where the complex exists as ~97% in the oxygenated form the ^{1}H NMR spectrum contracts within the normal 10-ppm range and the magnetic moment falls close to zero (0.6 μ_B). This low-spin six-coordinate iron(II) dioxygen adduct provides evidence therefore that such a configuration is possible and therefore that the $Fe^{II}O_2$ unit is not represented by Fe^{III}/O_2^- with its formal two unpaired electrons but rather that strong antiferromagnetic coupling must

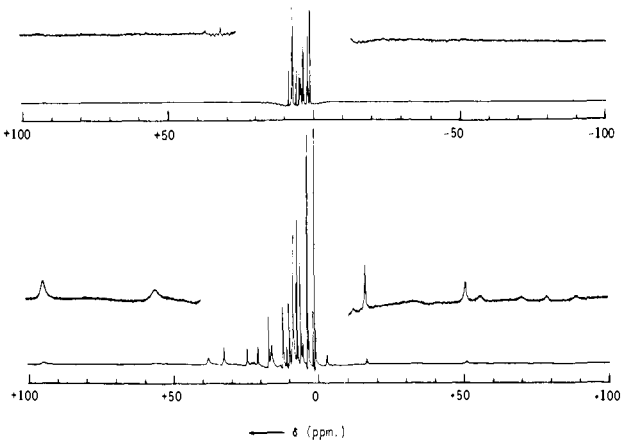

Figure 13. Lower spectrum: ^{1}H NMR spectrum of I, R^1 = *m*-xylylene, $R^2 = CH_2C_6H_5$, $R^3 = C_6H_5$, in $C_5^2H_5N$ at 253 K. Upper spectrum: same spectrum after exposure to 752 torr O_2 for 200 s.[33]

exist if indeed the iron–oxygen unit is polarized in this way.[38]

Conclusions

The syntheses and characterization of a wide range of new iron(II) lacunar complexes is reported, and they have been shown to be remarkable reversible dioxygen carriers. Binding constants for dioxygen span a wide range, dependent on substituent variations, and the longevity of the reversible behavior is likewise controlled. One heavily substituted complex reversibly binds O_2 at 20 °C in nonaqueous solvents, and even at 37 °C considerable reversibility persists. The systematic improvement in both control of the magnitude of K_{O_2} and stability toward autoxidation reported here lead us to expect that further rational alteration of lacunar structure and substituents will lead to reversible dioxygen carriers of iron(II) with truly remarkable perseverance and utility.[6] Although the reaction is undesirable for the present purposes, the exact mechanism of autoxidation of the FeO_2 adducts is the subject of other studies and has provided a bonus by revealing extremely interesting iron/reduced dioxygen species with many similarities to the heme protein cytochrome P450 system.[33] Our investigations in this area will be the subject of a forthcoming publication.

Acknowledgment. The support of the National Science Foundation is gratefully acknowledged. We also thank M. Y. Chavan for providing some of the electrochemical data on the iron(II) complexes, Dr. R. A. Wilkins for assistance with the gas uptake experiments, and T. Meade for assistance with ^{1}H NMR measurements.

Registry No. I(R^1 = *m*-xylylene; R^2 = H; R^3 = CH_3; B = Cl)·Cl·$2CH_3OH$, 87114-59-8; I(R^1 = *m*-xylylene; R^2 = CH_3; R^3 = CH_3; B = Cl)·PF_6, 84109-43-3; I(R^1 = *m*-xylylene; R^2 = CH_3; R^3 = C_6H_5; B = CH_3CN)·$2PF_6$, 84117-47-5; I(R^1 = *m*-xylylene; R^2 = $CH_2C_6H_5$; R^3 = CH_3; B = CH_3CN)·$2PF_6$, 84109-45-5; I(R^1 = *m*-xylylene; R^2 = $CH_2C_6H_5$; R^3 = C_6H_5; B = CH_3CN)·$2PF_6$, 84109-47-7; I(R^1 = *m*-xylylene; R^2 = CH_3; R^3 = C_7H_{15}; B = Cl)·PF_6, 87114-61-2; I(R^1 = *m*-xylylene; R^2 = Me; R^3 = *p*-$OMeC_6H_4$; B = Cl)·PF_6, 87114-63-4; I(R^1 = *m*-xylylene; R^2 = Me; R^3 = *p*-ClC_6H_4; B = Cl)·PF_6, 87114-65-6; I(R^1 = *m*-xylylene; R^2 = Me; R^3 = *p*-FC_6H_4; B = Cl)·PF_6, 87114-67-8; I(R^1 = $(CH_2)_4$; R^2 = H; R^3 = CH_3; B = Cl)·PF_6, 87114-69-0; I(R^1 = $(CH_2)_4$; R^2 = CH_3; R^3 = CH_3; B = Cl)·PF_6, 87114-71-4; I(R^1 = $(CH_2)_4$; R^2 = CH_3; R^3 = C_6H_5; B = Cl)·PF_6, 87114-73-6; I(R^1 = $(CH_2)_5$; R^2 = H; R^3 = CH_3; B = Cl)·Cl, 87114-74-7; I(R^1 = $(CH_2)_5$; R^2 = CH_3; R^3 = CH_3; B = Cl)·PF_6, 87114-76-9; I(R^1 = $(CH_2)_5$; R^2 = CH_3; R^3 = C_6H_5; B = Cl)·PF_6, 87114-78-1; I(R^1 = $(CH_2)_6$·R^2 = CH_3; R^3 = CH_3; B = Cl)·PF_6, 87114-80-5; I(R^1 = $CH_2)_6$; R^2 = CH_3; R^3 = C_6H_5; B = Cl)·PF_6, 87114-82-7; I(R^1 = $(CH_2)_6$; R^2 = $CH_2C_6H_5$; R^3 = C_6H_5; B = Cl)·PF_6, 87114-84-9; I(R^1 = $(CH_2)_6$; R^2 = H; R^3 = CH_3; B = Cl)·PF_6, 87114-86-1; I(R^1 = *p*-xylylene; R^2 = H; R^3 = CH_3, B = Cl)·PF_6, 87114-88-3; I(R^1 = C_7-fluorenylidene; R^2 = H; R^3 = CH_3; B = Cl)·PF_6, 87114-90-7; I(R^1 = *m*-xylylene; R^2 = CH_3; R^3 = CH_3; B = CH_3CN)·$2PF_6$, 87115-

(37) "CRC Handbook of Chemistry and Physics"; Vol. 53, The Chemical Rubber Company: Cleveland, OH, 1972; Vol. 53, p D-55.

(38) Makinen, M. W. "Biochemical and Clinical Aspects of Oxygen"; Academic Press: New York, 1979; p 143.

13-7; I(R^1 = *m*-xylylene; R^2 = CH_3; R^3 = CH_3; B = py)·2PF_6, 87114-92-9; I(R^1 = *m*-xylylene; R^2 = CH_3; R^3 = CH_3, B = 1-Mim)·PF_6, 87114-93-0; I(R^1 = *m*-xylylene; R^2 = $CH_2C_6H_5$; R^3 = CH_3; B = py)·2PF_6, 87114-95-2; I(R^1 = *m*-xylylene; R^2 = CH_3; R^3 = *n*-C_7H_{15}, B = py)·2PF_6, 87114-97-4; I(R′ = *m*-xylylene; R^2 = CH_3; R^3 = C_6H_5; B = py)·2PF_6, 87114-99-6; I(R′ = *m*-xylylene; R^2 = CH_3; R^3 = C_6H_5, B = 1-Mim)·2PF_6, 87115-01-3; I(R^1 = *m*-xylylene; R^2 = $CH_2C_6H_5$; R^3 = C_6H_5, B = py)·2PF_6, 87115-03-5; I(R′ = *m*-xylylene; R^2 = $CH_2C_6H_5$, R^3 = C_6H_5; B = 1-Mim)·2PF_6, 87115-05-7; I(R′ = *m*-xylylene; R^2 = CH_3; R^3 = *p*-$MeOC_6H_4$; B = py)·2PF_6, 87136-01-4; I(R^1 = *m*-xylylene; R^2 = CH_3; R^3 = *p*-ClC_6H_4; B = py)·2PF_6, 87115-07-9; I(R^1 = *m*-xylylene; R^2 = CH_3; R^3 = *p*-FC_6H_4; B = py)·2PF_6, 87115-09-1; I(R^1 = $(CH_2)_5$;R^2 = CH_3; R^3 = C_6H_5; B = py)·2PF_6, 87115-11-5; H_2O, 7732-18-5; bis(acetonitrile)iron(II) chloride, 87114-91-8; bis(pyridine)iron(II) chloride, 15616-26-9.

Supplementary Material Available: Atomic coordinates and calculated and observed structure factors for both structures (29 pages). Ordering information is given on any current masthead page.

X-ray Absorption Spectra and the Coordination Number of Zn and Co Carbonic Anhydrase as a Function of pH and Inhibitor Binding

Vittal Yachandra,[†] Linda Powers,[‡] and Thomas G. Spiro*[†]

Contribution from the Department of Chemistry, Princeton University, Princeton, New Jersey 08544, and Bell Laboratories, Murray Hill, New Jersey 07974.
Received January 13, 1983

Abstract: X-ray absorption spectra are reported for native (Zn) and Co-reconstituted bovine carbonic anhydrase (CA), prepared at several pH values across the acid–alkaline transition and in the presence of inhibitors (acetazolamide, imidazole, acetate, HCO_3^-, NO_3^-, Cl^-, CN^-, OCN^-, SCN^-). The extended fine structure (EXAFS) was analyzed by filtering the first-shell contribution and was compared with a series of model compounds of known structure having various coordination numbers. Co-CA showed variable coordination, as revealed by the calculated number of scatterers and by the average bond distance: four-coordination for the alkaline form and for complexes with CN^- and acetazolamide, and five-coordination for the acid form and for complexes with acetate and bicarbonate. For Zn-CA, however, the average coordination number is independent of pH, or of inhibitor binding, and is judged to be four from the relatively short ~2.01-Å average first-shell distance, although the EXAFS-determined average coordination numbers were slightly higher and are less reliable than the distance as monitors of the Zn coordination. Two-atom fits to the filtered first-shell EXAFS data improved the agreement for Zn-CA, with pairs of distances suggesting a ~0.1-Å spread in the Zn–ligand bond lengths, but no improvement was obtained for Co-CA. All of the EXAFS Fourier transforms showed the outer-shell peaks attributable to imidazole ring atoms, at constant intervals from the first-shell peak, implying no alterations in the angle of the imidazole rings relative to the metal–imidazole bonds. The K-edge spectra showed prominent 1s → 3d absorption bands for four-coordinate Co-CA complexes, reflecting 4p–3d mixing in near-tetrahedral geometry; the band is attenuated in the five-coordinated species. The main Co edge peak is broader for the four-coordinate species. The Zn edge peak is distinctively split in Zn-CA, as it is in some four-coordinate Zn model compounds, possibly due to 4p, 4d, and/or 5p mixing. The energy of the second component decreases slightly as the pH is raised, following the pK_a for enzyme activation; the direction is that expected for ionization of a Zn-bound group, presumably H_2O. The Zn- and Co-CA coordination states are discussed in relation to the enzyme mechanism.

We have applied X-ray absorption spectroscopy to probe the coordination environment of the metal ion in zinc (native) and cobalt (reconstituted) carbonic anhydrase. This enzyme[1] is of fundamental biological importance, since it catalyzes the hydration–dehydration reaction of CO_2

$$CO_2 + H_2O \rightarrow HCO_3^- + H^+$$

Intensive structural and kinetic studies by many investigators[2] have shed much light on the enzyme, but key elements of the mechanism remain the subject of controversy.

X-ray crystallography[3] has established that the Zn^{2+} ion, which is essential for catalysis, is held by three histidine ligands and is coordinated by one, or possibly two, water molecules. The enzyme is active only in its alkaline form, and is inhibited by monovalent anions, which bind to the acid form.[1,4] The acid–alkaline transition has a pK_a of ~7, although exclusion of anions, including the commonly used SO_4^{2-}, appears to lower the intrinsic pK_a to ~5.[1,5] Zinc can be removed and replaced by other metal ions,[1] but only Co^{2+} gives significant CO_2 hydration activity, at a level ~50% of that of native enzyme. The visible absorption spectrum of the Co^{2+} enzyme changes markedly through the acid–alkaline transition and in response to inhibitor binding. The spectra are decidedly nonoctahedral in character, but they have otherwise been difficult to interpret in terms of coordination number and geometry. Only the tight-binding inhibitors CN^- and aromatic sulfonamides give tetrahedral-looking spectra, other forms of the enzyme giving spectra of less regular appearance. A weak band in the 1400-nm region has been interpreted by Bertini et al.[6] as arising from a five-coordinate structure. It is present in complexes with weakly binding inhibitors such as acetate, SCN^-, and NO_3^-, but appears to be lacking in the acid or alkaline form of the uncomplexed enzyme, suggesting four-coordination.[6] The acid–alkaline spectral change is mimicked by the Co^{2+} complex of [tris(3,5-dimethyl-1-pyrazolyl)methyl]amine, which has four N ligands and H_2O at a fifth position; the complex has a pK_a of ~9.[7]

[†] Princeton University.
[‡] Bell Laboratories.

(1) See Lindskog (Lindskog, S. In "Zinc Proteins"; Spiro, T. G., Ed.; Wiley: New York, 1982; Chapter 3 (in press)) for a current review.
(2) "Biophysics and Physiology of Carbon Dioxide"; Bauer, C., Gros, G., Bartels, H., Eds.; Springer Verlag: West Berlin, 1980.
(3) Kannan, K. K., in ref 2.
(4) Coleman, J. E., in ref 2.
(5) Koenig, S. H.; Brown, R. D.; Jacob, G. S., in ref 2, p 238.
(6) Bertini, I.; Canti, G.; Luchinat, C.; Scozzafava, A. *J. Am. Chem. Soc.* **1978**, *100*, 4873.

0002-7863/83/1505-6596$01.50/0